




Theoretical Characterization of Indentation Depth-Dependent Creep Behavior of CoCrFeNiAl_{0.3} High-Entropy Alloy

Lu Meng^{1,2} · Weiling Cui³ · Buyun Su^{1,2} · Xuefeng Shu^{1,2}  · Gesheng Xiao^{1,2}

Received: 4 May 2022 / Revised: 19 August 2022 / Accepted: 22 August 2022 / Published online: 20 September 2022
© The Chinese Society of Theoretical and Applied Mechanics 2022

Abstract

The effects of indentation loading depth and dynamic pre-compression on the creep behavior of CoCrFeNiAl_{0.3} high-entropy alloy (HEA) were studied through a series of indentation creep tests. Results show that the creep displacement, creep stress exponent and creep strain rate are all sensitive to loading depth. A phenomenological model based on the holding time and loading depth was established by studying the characteristic relation between the loading depth and the creep displacement of CoCrFeNiAl_{0.3} HEA. The phenomenological model was used to analyze the creep behavior of the alloy under dynamic pre-compression (i.e., dynamic compressive deformation caused by Hopkinson bar impact).

Keywords High-entropy alloy · Creep behavior · Phenomenological model · Indentation depth-dependence · Dynamic pre-compression

1 Introduction

Hitherto, CoCrFeNiAl_{0.3} high-entropy alloys (HEAs) have good application prospects in advanced fields such as aero-engine turbine blades, rocket nozzles, marine vessels and high-frequency communicator [1]. With the booming development of nanoindentation instrument, the study of nano-mechanics has risen rapidly [2–4]. Mechanical parameters such as indentation hardness, fracture toughness and strain hardening exponent can be accessed through in situ micro/nanoindentation test, and the displacement–time relation under constant stress is also supposed to be a proper phenomenon for the nanoindentation investigation [5]. Creep is the phenomenon that the strain of material increases with time under constant stress [6]. The existing research focuses

on the effect of strain rate on creep behavior, for instance, Hu et al. [7] showed that the creep behavior is sensitive to loading rate. At high loading rates, the interaction between dislocations and twins is enhanced to produce high-density statistical storage dislocations. The rapid absorption of these statistically stored dislocations (SSDs) in the loading state and the new nucleation dislocations in the holding state result in a high initial creep rate. In contrast, few dislocations can be stored at low loading rates, and creep behavior is mainly dominated by grain boundary sliding. But the creep behavior under different loads or depths has rarely been studied in detail. At present, Zhou et al. [8] have conducted indentation creep tests under different loads or depths, and used empirical models proposed by some authors [9, 10] to fit the indentation creep curves to analyze the creep behavior changes under different conditions. However, the correlation between fitting parameters and creep characteristics is not clear, and there is no quantitative analysis of creep behavior. Besides, the creep strain of metals is caused by dislocation motion and diffusion mechanism, which are primarily controlled by dislocations, solute-matrix bonding and precipitates. And the dynamic deformation of HEAs has been reported [11, 12] as additive mechanisms such as twinning, dislocation, shear banding and phase transformation, which usually occurs in conventional metals and alloys at high strain rates (strain rate > 10³ s⁻¹) [13]. Therefore, it is vital to clearly under-

✉ Xuefeng Shu
shuxuefeng@tyut.edu.cn
Gesheng Xiao
xiaogesheng@tyut.edu.cn

¹ Institute of Applied Mechanics, College of Mechanical and Vehicle Engineering, Taiyuan University of Technology, Taiyuan 030024, China

² Shanxi Key Laboratory of Material Strength and Structural Impact, Taiyuan 030024, China

³ College of Biomedical Engineering, Taiyuan University of Technology, Taiyuan 030024, China

stand the effect of dynamic deformation on indentation creep behavior.

The purpose of this work is to establish a phenomenological model to determine the creep curve via given holding time and loading depth, and quantitatively predict and characterize the indentation creep behavior of CoCrFeNiAl_{0.3} HEA at different loading depths. Moreover, the phenomenological model is applied to the creep behavior of CoCrFeNiAl_{0.3} HEA subjected to dynamic loading.

2 Experimental Procedure and Characterization Method

2.1 Experiment

Alloy ingots with a nominal composition of as-cast CoCrFeNiAl_{0.3} HEA were prepared by arc-melting pure elements (purity > 99.9 weight percent) in a Ti-gettered high-purity argon atmosphere. The alloy was re-melted four times and annealed at 1100 °C for 1 h in order to obtain chemical homogeneity and eliminate residual stress. The alloy rods with 6.9-mm diameter and 6-mm height by the copper-mold suction casting were marked as specimen 1 and specimen 2, respectively. Additionally, the corresponding result of crystal structure analysis via X-ray diffraction (XRD) is shown in Fig. 1a, which indicates that typical FCC crystal structure mainly presents in CoCrFeNiAl_{0.3} HEA.

The split-Hopkinson pressure bar (SHPB) device was used to perform a dynamic experiment with a strain rate of 10^3 s^{-1} for specimen 2 at room temperature. The true stress versus strain and strain versus strain rate curves for CoCrFeNiAl_{0.3} HEA under dynamic compression are plotted in Fig. 1b, and the inset shows the size states of the material before and after dynamic compression. The alloy was continuously compressed without a failure even at the strain of 18.8%. Specimen 2 with pre-compression was cut radially through the wire electrical discharge machining (WEDM) for comparison with specimen 1. The specimens were pre-set and vertically fixed via inlay powder, and then the three planes of the tested specimens used in the micro-indentation test were polished into a mirror-like state with a series of SiC sand paper (#800, 1000, 1200, 1500, 2000, 2500, and 3000), diamond suspensions and electrolytic polishing, as shown in Fig. 1c.

Micro-indentation creep tests were carried out using the Agilent Nano Indenter G200 test system with force and displacement being 50 nN and 0.01 nm, respectively. The tests were performed using the triangular pyramidal Berkovich diamond indenter in the strain rate-controlled mode via controlling the constant strain rate (\dot{P}/P) to be 0.05 s^{-1} . The

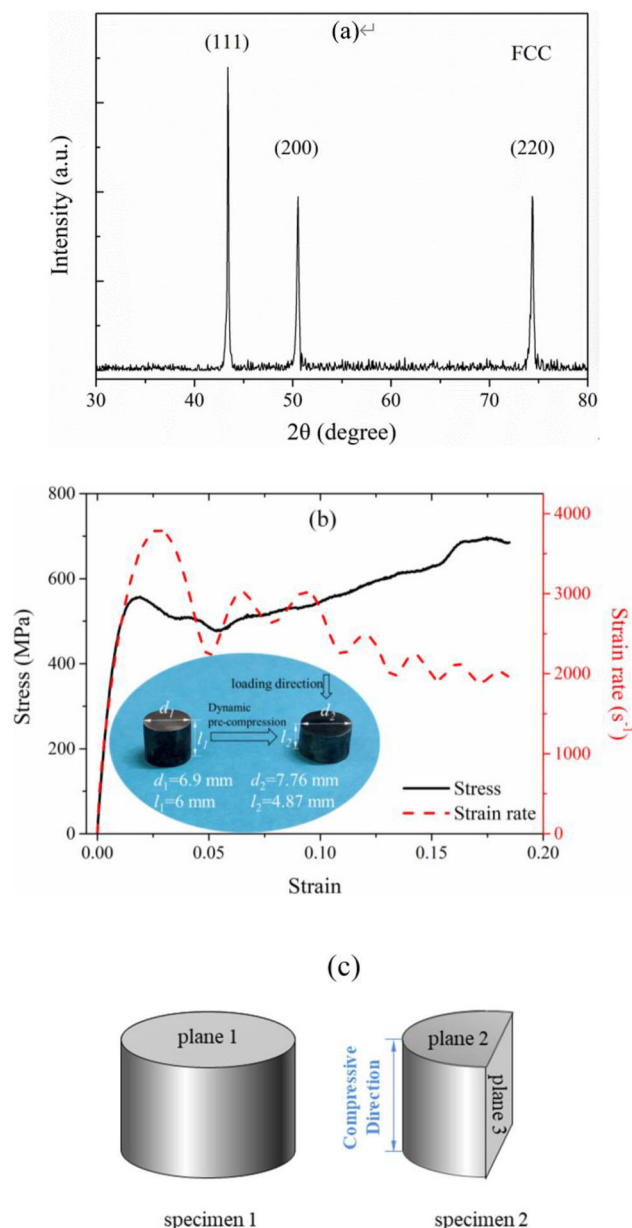


Fig. 1 Experimental preparation diagram of CoCrFeNiAl_{0.3} HEA: **a** XRD pattern; **b** specimen 1 without dynamic pre-compression and specimen 2 with dynamic pre-compression for micro-indentation test; **c** the stress–strain and strain rate–strain curves under dynamic loading

six different peak depths were set as 500, 1000, 1500, 2000, 2500 and 3000 nm, respectively, with the holding time of 1800s. Creep experiments were conducted at room temperature, then the peak load was decreased to $0.1P_{\max}$ within 2 s for thermal drift correction. In addition, three independent indentations were made for each condition.

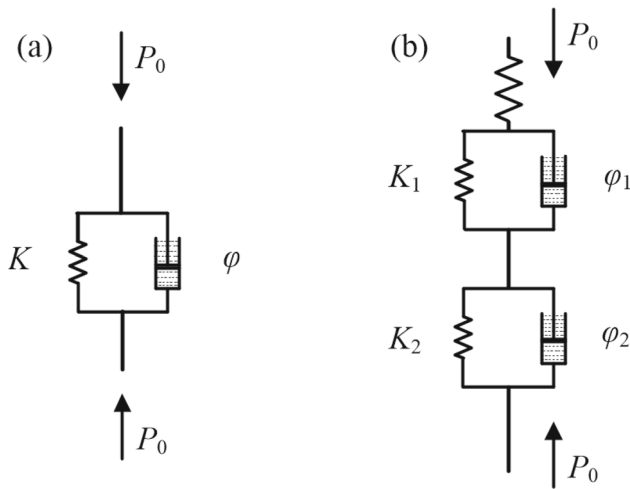


Fig. 2 a Two-element Kelvin model; b generalized Kelvin model

2.2 Phenomenological Model

On account of the non-destructive nature of micro-indentation test, its creep curve shows two stages [14]. The initial creep displacement increases rapidly, and the creep rate decreases rapidly, which is the transient-state creep. The latter creep displacement increases linearly, and the creep rate is stable, which is the quasi-steady-state creep. Yang et al. [10] proposed a generalized Kelvin model (Fig. 2b) based on the principle of series and parallel connection of springs and dashpots, which has been one of the most commonly used models to describe the creep behavior of different materials under indentation test. Through defining $\sigma_0 = P_0/A_0$ and $\varepsilon = \Delta h/h_{in}$, the stress-strain relationship of the Kelvin model is transformed into the relationship between indentation load and indentation depth, that is, $\Delta h = \frac{P_0}{K_i}(1 - e^{-K_i t/\varphi_i})$. Thereinto, Δh represents the creep displacement, P_0 is the constant indentation load for the creep test, K_i and φ_i are constants related to the spring constant and the viscosity coefficient of the dashpot, respectively, and they can be substituted by $P_0/K_i = h_i$, $\varphi_i/K_i = \tau_i$ ($i = 1, 2$) and written as $\Delta h = h_1(1 - e^{-t/\tau_1}) + h_2(1 - e^{-t/\tau_2})$. So the indentation depth based on the Kelvin model to characterize the creep behavior is expressed as

$$h_i(t) = h_0 + \Delta h = h_0 + h_1(1 - e^{-t/\tau_1}) + h_2(1 - e^{-t/\tau_2}) \tag{1a}$$

where h_i and τ_i represent the indentation depth and the retardation time for the i th Kelvin element, respectively, as function of indentation loading depth for selected materials. For the creep behavior of materials, h_0 represents the total depth of indentation loading stage. When loading to the loading depth set ahead, the loading cannot be stopped immediately due to the loading rate, so h_0 is assumed to

increase linearly with the depth set, as shown in Eq. (1b.1). h_1 and τ_1 characterize the transient-state creep. For the reason that the transient creep occurs when the material experiences hardening through changes in the dislocation substructure, and the creep displacement increases rapidly with the holding time, h_1 and τ_1 are assumed to have a linear relation with the loading depth, as shown in Eq. (1b.2). h_2 and τ_2 characterize the quasi-steady-state creep. At this stage, the hardening is balanced by dynamic recovery (e.g., dislocation annihilation), which is manifested as the creep displacement increases slowly with the increase in the holding time [15]. Different from the characteristic of the slowing down of growth trend of creep displacement, we assume that h_2 and τ_2 have an exponential relation with the loading depth in Eq. (1b.3), as summarized below

$$h_0(h) = a + ch \tag{1b.1}$$

$$h_1(h) = z + rh, \quad \tau_1(h) = g + jh \tag{1b.2}$$

$$h_2(h) = be^{-h/d} + nh + m, \quad \tau_2(h) = qe^{-h/p} + uh + w \tag{1b.3}$$

where h is the indentation loading depth, $a, c, z, r, g, j, b, d, n, m, q, p, u,$ and w are the material creep parameters related to the loading depth obtained by the above formulae combined with the fitting parameters of the creep curves. The phenomenological model (Eq. 1) with all parameters determined can predict the creep curves of the materials at different loading depths.

To further investigate the creep mechanism of materials under different loading depths, the creep stress exponents were calculated. It is well-known that creep stress exponent of quasi-steady state is the crucial indicator for inferring the material creep mechanism. The empirical power-law creep equation that characterizes quasi-steady creep process is as follows [16]:

$$\dot{\varepsilon} = B\sigma^n \exp(-Q/RT) \tag{2}$$

where $\dot{\varepsilon}$ is the creep strain rate, B is the Boltzmann constant, R is the gas molar constant, n is the creep stress exponent, σ is the applied stress, Q is the activation energy, and T is absolute temperature. The above equation at room temperature can be simplified as $\dot{\varepsilon} = \sigma^n$, which is represented as the slope of the typical double logarithmic curve of creep strain rate versus hardness

$$n = \frac{\partial \ln \dot{\varepsilon}}{\partial \ln H} \tag{3}$$

During self-similar indentation creep, $\dot{\varepsilon}$ in the depth-sensing indentation technique obeys the following relation [15]:

$$\dot{\varepsilon} = \frac{\dot{h}}{h} = \frac{1}{h} \frac{dh}{dt} \quad (4)$$

where h is the instantaneous displacement of indenter, t is time, and dh/dt is the displacement rate, which can be substituted by empirical Eq. (1) and expressed as

$$\dot{\varepsilon}(h, t) = \frac{(h_1/\tau_1)e^{-t/\tau_1} + (h_2/\tau_2)e^{-t/\tau_2}}{h_0 + h_1(1 - e^{-t/\tau_1}) + h_2(1 - e^{-t/\tau_2})} \quad (5)$$

For an indenter with known geometry such as the Berkovich tip used, the hardness H , indentation load P , contact area A_c and contact depth h_c of CoCrFeNiAl_{0.3} HEA under micro-indentation test are defined as follows [17]:

$$H = \frac{P}{A_c} \quad (6)$$

$$A_c = 24.56h_c^2 \quad (7)$$

$$h_c = h_{\max} - \varepsilon \frac{P_{\max}}{S} \quad (8)$$

where ε is a constant related to the shape of the indenter ($\varepsilon = 0.72$) [17]. h_{\max} , P_{\max} and S are the maximum loading depth, the maximum indentation load, and the contact stiffness, respectively. According to the principle of micro-indentation test, the relationship between these three mechanical parameters and loading depth can be established, respectively, as shown below:

$$h_{\max} = h_t(h, t) \quad (9)$$

$$P_{\max} = \omega h^v \quad (10)$$

$$S = \beta h \quad (11)$$

Combining Eqs. (6)–(8), the relation between the measured hardness and loading depth during creep process is derived as follows:

$$H = \frac{\omega h_0^v}{24.56 \cdot \left[h_t(h, t) - \varepsilon \omega h_0^{v-1} / \beta \right]} \quad (12)$$

Substituting Eqs. (5)–(6) and (8) into Eq. (12) yields the following:

$$n = \frac{\partial \ln \dot{\varepsilon}(h, t)}{\partial \ln H(h, t)} = \frac{1}{2} \frac{\left[\frac{(h_1/\tau_1^2)e^{-t/\tau_1} + (h_2/\tau_2^2)e^{-t/\tau_2}}{(h_1/\tau_1)e^{-t/\tau_1} + (h_2/\tau_2)e^{-t/\tau_2}} + \frac{(h_1/\tau_1)e^{-t/\tau_1} + (h_2/\tau_2)e^{-t/\tau_2}}{h_0 + h_1(1 - e^{-t/\tau_1}) + h_2(1 - e^{-t/\tau_2})} \right]}{\left[\frac{(h_1/\tau_1)e^{-t/\tau_1} + (h_2/\tau_2)e^{-t/\tau_2}}{h_0 + h_1(1 - e^{-t/\tau_1}) + h_2(1 - e^{-t/\tau_2})} - (\varepsilon\omega/\beta)h_0^{v-1} \right]} \quad (13)$$

Substituting all material parameters into Eq. (13) can predict n under different loading conditions.

3 Results and Discussion

3.1 Indentation Creep Behavior of CoCrFeNiAl_{0.3} HEA Without Pre-compression

Figure 3a shows the representative load–displacement (P – h) curves of creep tests with various indentation loading depths ranging from 1000 to 2500 nm for the alloy, and the platforms appearing on each curve represent the load-holding period. The creep displacement versus holding time data and corresponding fitting results are shown in Fig. 3b. It is found that the fitting protocol in Eq. (1a) can accurately fit the creep curves for four different loading depths. Substituting the fitting parameters (listed in Table 1) into Eq. (1b) can obtain the creep parameters, the fitting process of which is shown in Fig. 3c, and the results are listed in Table 2. The creep curves of the HEA at loading depths of 500 and 3000 nm were predicted using the phenomenological model with all parameters determined and compared with the experimental results in Fig. 4. The results display that the phenomenological and experimental results have the largest displacement deviation (the corresponding deviations are 0.18% and 0.35%, respectively) when the holding time is 1800s. Obviously, the phenomenological results are in good accordance with experimental observations and the creep phenomenological model (Eq. 1) can accurately predict the creep curve at a given loading depth.

The material parameters determined via Eqs. (10)–(11) (see Fig. 5a, b) are substituted into Eq. (5) to plot the creep strain rate at each loading depth in Fig. 5c. The strain rate decreases rapidly in the transient-state stage, and reaches a stable value approaching 10^{-5} s^{-1} with prolonged holding time until the creep enters the quasi-steady state. The Coble diffusion creep mechanism only occurs when the creep strain rate is lower than 10^{-6} s^{-1} [14], while the minimum strain rate of $\sim 10^{-5} \text{ s}^{-1}$ in the experiment is much larger than the critical value. Therefore, Coble diffusion creep is not the operative mechanism for micro-indentation creep behav-

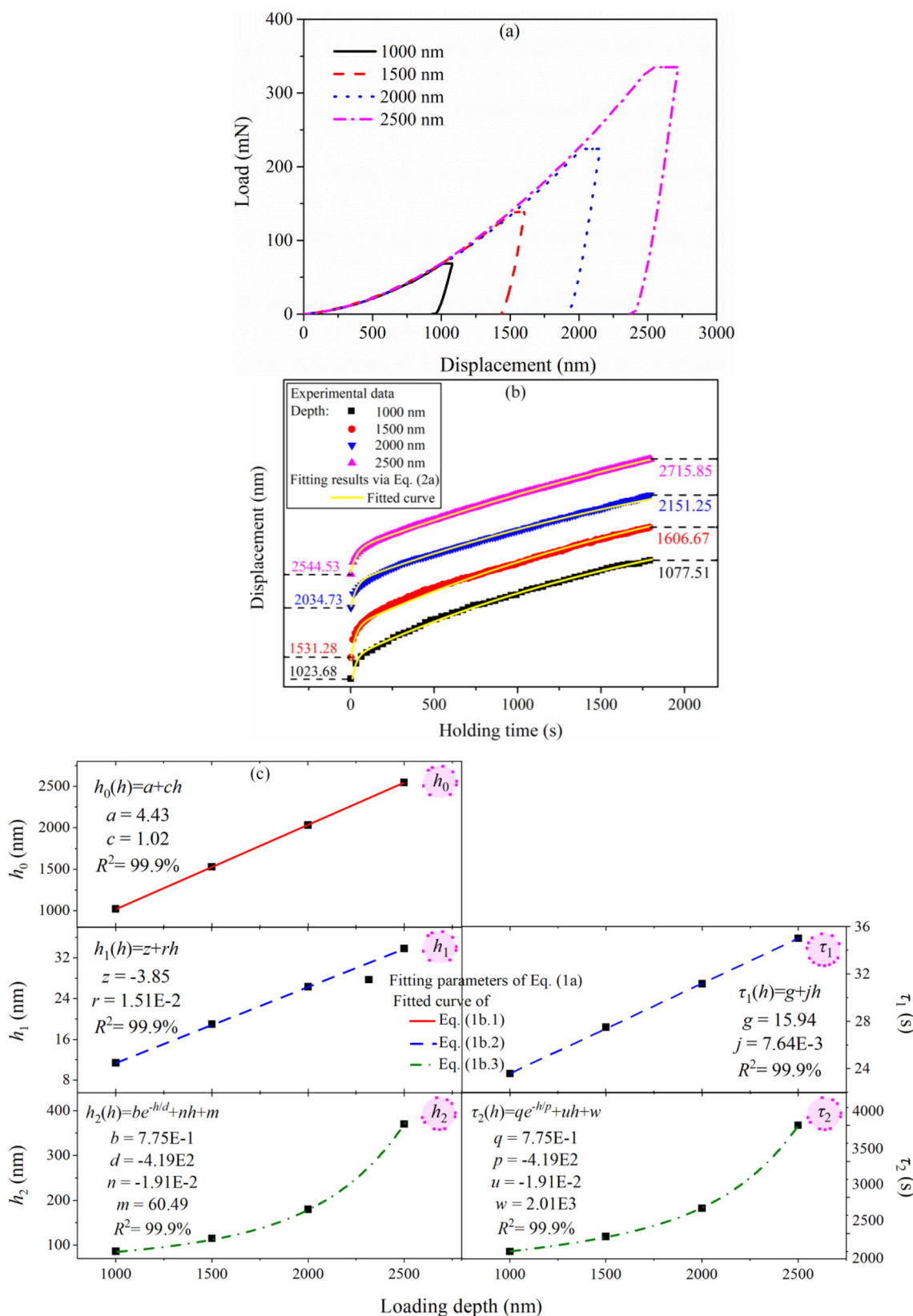


Fig. 3 Indentation test curves of CoCrFeNiAl_{0.3} HEA without pre-compression: **a** load–displacement curves; **b** creep displacement curves and the corresponding fitting results; **c** fitting curves of 14 creep parameters in Eq. (1b)

Table 1 Fitting parameters in Eq. (2a)

Fitting parameters	Loading depth (nm)			
	1000	1500	2000	2500
h_0 (nm)	1021.4	1530.1	2034.9	2547.2
h_1 (nm)	11.8	19.0	26.0	33.8
τ_1 (s)	23.7	27.5	31.1	35.0
h_2 (nm)	80.1	115.0	180.0	370.1
τ_2 (s)	2165.7	2537.3	2750.1	4000.0
R^2 (%)	99.8	99.3	99.6	99.9

Table 2 Creep parameters in Eq. (2b) for plane 1

A	c	z	r	g	j	b
4.43	1.02	-3.85	1.51E-2	15.94	7.64E-3	7.75E-1
d	n	m	q	p	u	w
-	1.91E-2	60.49	2.95	-	2.15E-1	2.01E3
4.29E2				4.05E2		

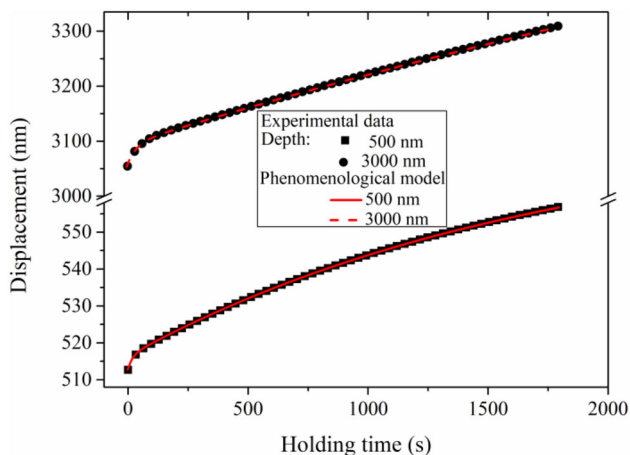


Fig. 4 Experimental data and corresponding phenomenological curves under different loading depths

ior. Furthermore, substituting three fitting parameters and 14 creep parameters (Table 2) into the phenomenological model of Eq. (13) and setting the holding time to 1800s, the phenomenological n at all loading depths can be plotted. To sum up, Fig. 5d plots the experimental data of n (black dots) and $\dot{\epsilon}$ (blue dots) varying with the loading depth, as well as the comparison between the experimental and phenomenological (red curve) values of n . It is observed that the phenomenological model of stress exponent predicts accurately. Hence, it is confirmed that the phenomenological model can predict the creep curve and n over all loading depths with the determination of the two related sets of parameters.

On the other hand, n and $\dot{\epsilon}$ reach their extreme values at the same loading depth. Combining the change trends of $\dot{\epsilon}$ and n can estimate the change of creep mechanism with loading

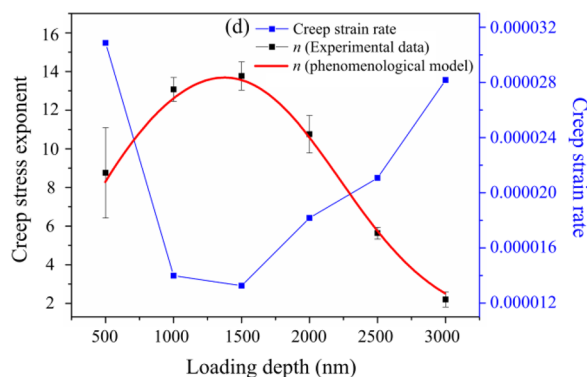
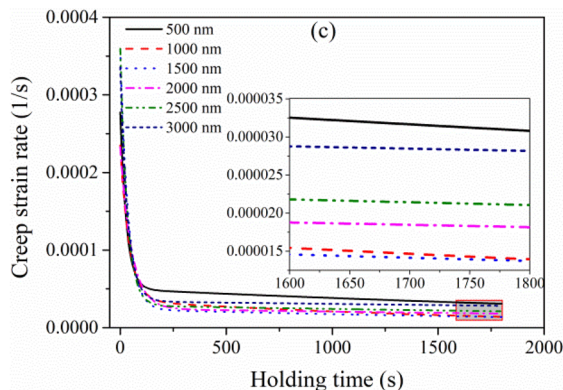
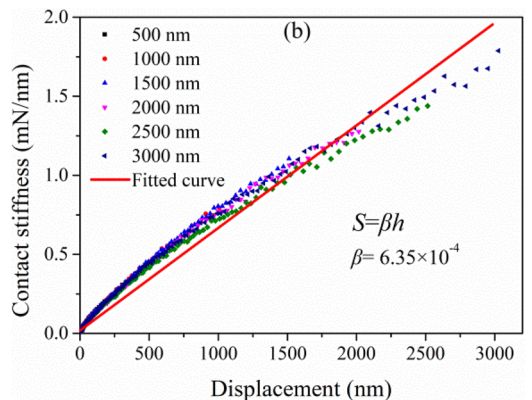
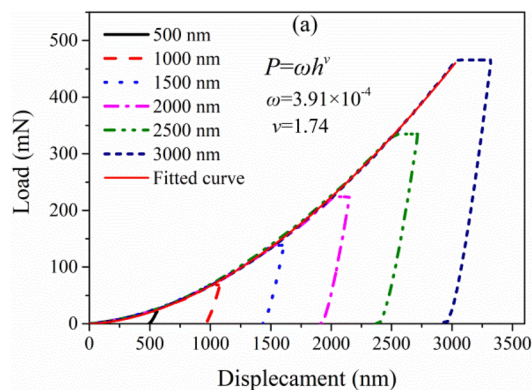


Fig. 5 **a** Fitting result of P - h curve; **b** the linear fitting result of contact stiffness-depth curve; **c** creep strain rate versus holding time; **d** experimental and the corresponding phenomenological creep stress exponent n , and the changes of n and creep strain rate $\dot{\epsilon}$ at different loading depths

Table 3 Fitting parameters in Eq. (2a) for plane 2 and plane 3

Parameters	Plane 2				Plane 3			
	Loading depth (nm)				Loading depth (nm)			
	1000	1500	2000	2500	1000	1500	2000	2500
h_0 (nm)	1018.5	1529.5	2042.7	2549.0	1019.9	1525.3	2042.9	2539.3
h_1 (nm)	6.2	10.5	14.7	18.8	5.4	9.6	13.9	18.0
τ_1 (s)	24.3	28.3	32.6	36.9	30.4	34.9	39.5	44.4
h_2 (nm)	54.0	89.6	151.1	327.9	12.8	39.3	95.0	220.5
τ_2 (s)	2150.0	2226.1	2632.2	3737.4	967.0	1275.0	2042.4	3600.0
R^2 (%)	99.4	99.9	99.6	99.9	98.6	98.9	99.5	99.6

depth [14]. Cao et al. [18] pointed out that high $\dot{\epsilon}$ and low n indicate that diffusion and slip are the main creep mechanisms, and Wang et al. [19] introduced the self-diffusion along the tip-specimen mechanism, which is generally considered occurring when the loading depth is less than 30 nm. Given that the smallest loading depth reached by the creep tests in this section is much higher than this critical value, the grain boundary slip is the dominant creep mechanism at 500 nm (high $\dot{\epsilon}$ and low n). It is well known that self-diffusion, grain boundary and dislocation are the valid diffusion channels during creep deformation [18]. For the CoCrFeNiAl_{0.3} HEA with coarse grain sizes [20], the effect of grain boundary diffusion on creep behavior is not considered. As the loading depth increases to 1500 nm and the load increases, the high stress causes more dislocation nucleation, dislocation multiplication and dislocation slip in the local area, dislocation motion may be the operative mechanism [14]. Another strong evidence is that research of Zhou et al. [8] showed that when $n > 3$, dislocation mechanism dominates the creep behavior. The maximum stress is applied when the loading depth achieves 3000 nm. Sun et al. [21] pointed out that the creep dislocation activities under high stress dominate the mechanism and cause a higher creep strain rate. When the depth continues to increase to 3000 nm, the holding load reaches its maximum, and the dislocation mechanism under high stress is considered to be dominant. However, at a depth of 3000 nm, n decreases to 2.1, Zhou et al. pointed out that $n = 2$ for grain boundary slip. The reason might be that the new dislocations generated during the creep deformation hinder the sliding and entanglement of the original movable dislocations, and the dislocation block obstructs the dislocation motion (including slip and climb) [20]. Consequently, grain boundary slip and dislocation motion are the creep mechanisms at the loading depth of 3000 nm.

3.2 Indentation Creep Behavior of CoCrFeNiAl_{0.3} HEA with Pre-compression

Usually, the creep strain of alloy is triggered by the dislocation motion and diffusion mechanism. Applying pre-

Table 4 Creep parameters in Eq. (2b) for plane 2 and plane 3

Creep parameters for plane 2							
a	c	z	r	g	j	b	
7.44	1.02	- 2.01	8.4E-3	15.4	8.6E-3	3.36E-1	
d	n	m	q	p	u	w	
3.86E2	3.62E-2	18.97	21.12	2.51E2	-	2.11E3 1.35E-1	
Creep parameters for plane 3							
a	c	z	r	g	j	b	
8.24	1.01	- 3.14	8.52E-3	20.94	9.39E-3	9.04E-2	
d	n	m	q	p	u	w	
3.35E2	3.14E-2	- 12.06	201.91	8.54E2	-	5.92E2 3.14E-1	

compression that causes plastic deformation can cause dislocation loops, spiral dislocations and even certain phase precipitates. Xu et al. [22] found that the large is the pre-strain, the more are the dislocation forms. Hence, the validity of the creep model in Sect. 3.1 can be verified again by studying the creep behavior of the CoCrFeNiAl_{0.3} HEA with pre-compression. Indentation creep tests were carried out on the axial and transverse compression planes. In this paper, these are marked as plane 2 in the compression direction and plane 3 in the transverse direction. According to Sect. 3.1, the corresponding parameters of plane 2 and plane 3 are listed in Tables 3 and 4. The phenomenological model (Eq. 1) with all parameters determined can predict the creep curves of the two planes at different loading depths. Figure 6a, b shows the experimental data and the corresponding phenomenological results of the two planes at the loading depths of 500 and 3000 nm, respectively. (The corresponding deviations are 8.2% and 8.6%, respectively.) The phenomenological model in Sect. 3.1 still accurately predicts the indentation creep behavior of CoCrFeNiAl_{0.3} HEA even if the pre-compression is applied to it. Its effectiveness is thus confirmed.

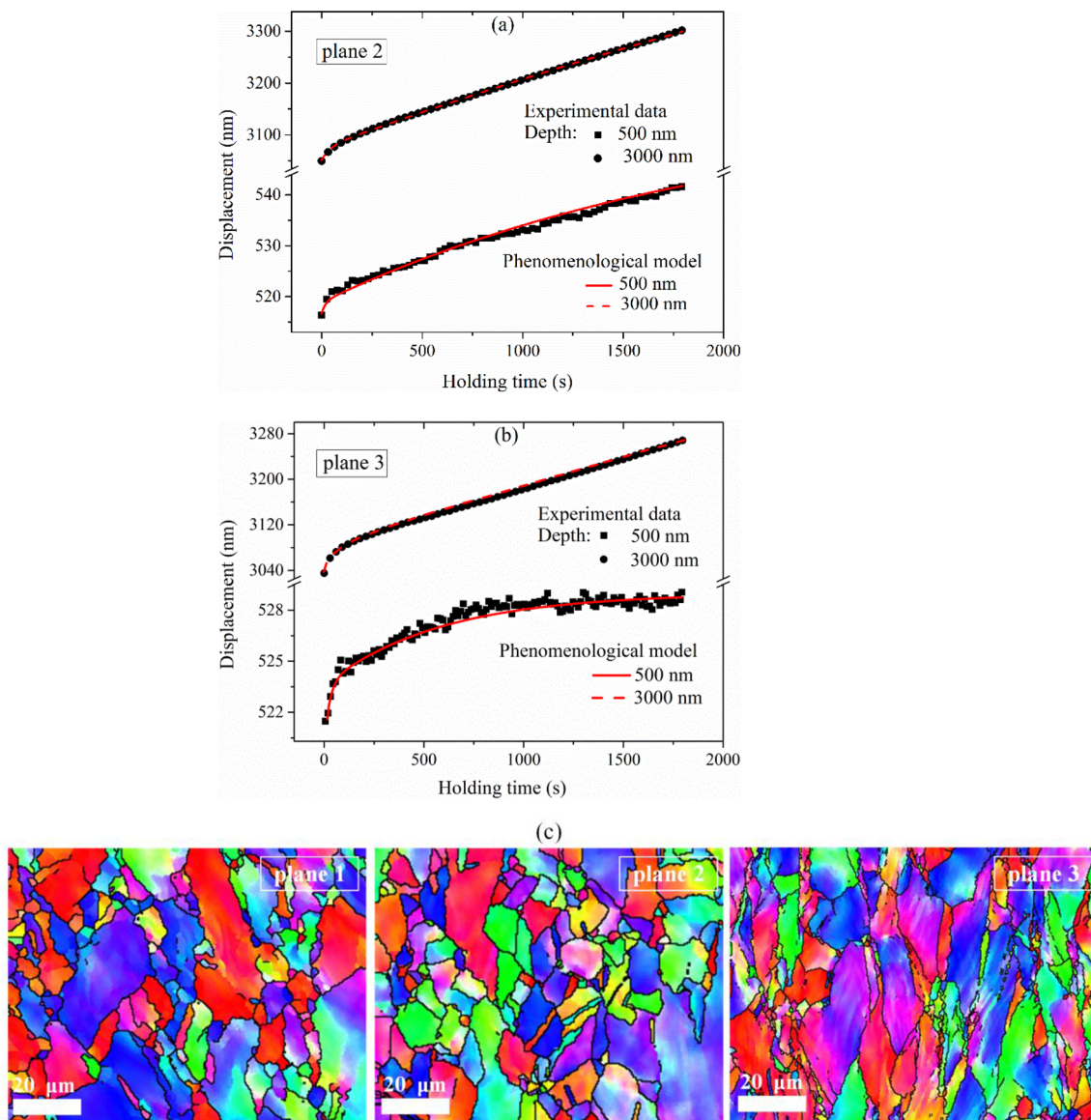


Fig. 6 CoCrFeNiAl_{0.3} HEA with pre-compression: experimental creep curves and corresponding phenomenological results of **a** plane 2, and **b** plane 3; **c** IPFs of EBSD test of plane 1 (without pre-compression), plane 2 (with pre-compression) and plane 3 (with pre-compression)

The comparisons of mechanical properties such as hardness, creep displacement and stress exponent under three operating conditions are summarized in Table 5. The increase in hardness of pre-compressed alloys can be explained from the following aspects. On account of dislocation evolution [12], the increase in dislocation density under dynamic loading is because the deformation time is too short for dislocation offset. The high dislocation density intensifies the interaction between dislocations, and the dislocations entangle one another to reach the dislocation forest state. Such dislocation strengthening mechanism improves the hardness. On the other hand, the electron backscattered diffraction (EBSD) test was performed using a JSN-700F field emission scanning electron microscope (SEM). The EBSD inverse polar figure

of surface morphology of plane 1 (CoCrFeNiAl_{0.3} HEA without pre-compression), plane 2 and plane 3 (CoCrFeNiAl_{0.3} HEA with pre-compression) are shown in Fig. 6c. It can be observed that the grain deformation of HEA subjected to dynamic loading is obvious inhomogeneous. Compared with the pre-compressed plane, the grains are subdivided by elongated strips on the transverse plane due to strong plastic deformation, which well-explains why the hardness of plane 2 is higher than that of plane 3.

The application of pre-compression has a significant effect on the creep behavior of CoCrFeNiAl_{0.3} HEA. After applying pre-compression, the creep displacement decreases at all loading depths. The difference in creep displacement is 58.8% when the loading depth is 500 nm and 11.2%

Table 5 Mechanical parameters of CoCrFeNiAl_{0.3} HEA under three operating conditions

	Without pre-compression	With pre-compression	
	Plane 1	Plane 2	Plane 3
Loading depth (nm)	Hardness (GPa)		
500	3.8	5.8	5.1
1000	3.1	5.1	4.7
1500	2.9	4.8	4.4
2000	2.8	4.4	4.3
2500	2.7	4.3	4.2
3000	2.6	4.2	3.7
	Creep displacement (nm)		
500	42.8	23.5	17.6
1000	53.1	27.0	21.4
1500	76.1	56.8	47.2
2000	107.6	85.6	78.7
2500	163.1	141.7	136.2
3000	264.9	243.9	235.3
	Stress exponent		
500	8.7	14.2	22.9
1000	13.1	21.2	28.8
1500	13.7	22.5	29.3
2000	10.7	12.9	15.9
2500	5.6	5.7	5.8
3000	2.1	2.2	2.3

when the loading depth is 3000 nm. The creep stress exponent n increases at all loading depths, and the difference in n is 61.9% when the loading depth is 500 nm and 22.8% when the loading depth is 3000 nm. The effect of pre-compression depends on the competition between pre-stress-induced dislocations and dislocation nucleation during indentation. At shallow indentation, preexisting dislocations dominate the deformation mechanism, and as the indentation depth increases, the competition for dislocation nucleation, movement and accumulation effects induced by the indenter is stronger than that for preexisting dislocations. Thus, the interference of the pre-compression on creep behavior is weakened with the increase in loading depth, which indicates that the pre-compression effect originates from the pre-compression-induced plasticity, scilicet, the dislocation [11, 23]. Overall, it is found that the pre-compression leads to numerous pre-dislocations in the alloy, and the preexisting dislocations increase the resistance to dislocation motion during the indentation creep test, thus improving the creep resistance of the CoCrFeNiAl_{0.3} HEA. Under dynamic loading conditions, the grains in the transverse plane are stretched as elongated strips along the transverse direction (perpendicular to the loading direction) compared to the loading

plane (see Fig. 6c). The elongated deformed grains have dense grain boundaries which hinder dislocation diffusion and motion. Therefore, in Table 5, the creep displacement of plane 3 is stably lower than that of plane 2, in other words, the creep resistance of plane 3 is stronger. This can be used as a reference to further understand the influence of macroscopic dynamic impact on the microscopic plastic deformation mechanism of high-entropy alloy and develop its excellent properties.

4 Conclusions

Micro-indentation creep tests are performed on CoCrFeNiAl_{0.3} HEA without and with dynamic pre-compression under different loading depths. All the creep parameters in the established creep behavior phenomenological model can be determined based on the creep curves of the alloy without pre-compression. Further, combining with the indentation experimental data, a phenomenological equation is determined to predict the stress exponent at different loading depths. The comparison shows that the phenomenological results of creep curve and stress exponent are consistent with the experimental data. Using the proposed phenomenological model to analyze the effect of dynamic pre-compression on the indentation creep behavior of CoCrFeNiAl_{0.3} HEA, the creep behavior shows sensitive to loading depth. Additionally, pre-compression promotes the creep resistance of CoCrFeNiAl_{0.3} HEA, and creep behaviors of the two planes are distinct due to different grain deformations of the compression plane and transverse plane under dynamic loading. The phenomenological model proposed under the micro-indentation creep test of the alloy without pre-compression is reasonable and reliable, and can be applied to predict and analyze the creep behavior of dynamic pre-compression alloy, which lays a foundation for the application of micro-indentation to obtain the influence of pre-deformation on the mechanical properties of CoCrFeNiAl_{0.3} HEA.

Acknowledgements The authors gratefully acknowledge financial support from the China Postdoctoral Science Foundation (Grant No. 2021M702605) and National Natural Science Foundation of China (Grant Nos. 12102287, 12102289, 11772217).

Authors' contributions LM contributed to conceptualization, methodology, experiment, data curation, original draft preparation, and writing; WC contributed to conceptualization and supervision; BS contributed to conceptualization and supervision; XS contributed to founding acquisition and supervision; GX contributed to founding acquisition, reviewing and editing.

Availability of Data and Materials The datasets used and analyzed during the current study are available from the corresponding author on reasonable request.

Declarations

Conflict of interest The authors declare that they have no known competing financial interests or personal relationships that could have appeared to influence the work reported in this paper.

References

1. Yeh JW, Chen YL, Lin SJ. High-entropy alloys—a new era of exploitation. *Mater Sci Forum*. 2007;560:1–9.
2. Fischer-Cripps AC. *Nanoindentation*. New York: Springer; 2011.
3. Meng L, Qiu J, Wang ZH, Liu RQ, Shu XF, Xiao GS. Indentation pop-in behavior of CoCrFeNiAl_{0.3} high-entropy alloy. *Mater Res Express*. 2020;6(12):1265d4.
4. Xiao GS, Yang XX, Qiu J, et al. Determination of power hardening elastoplastic constitutive relation of metals through indentation tests with plural indenters. *Mech Mater*. 2019;138:103173.
5. Lucas BN, Oliver WC. Indentation power-law creep of high-purity indium. *Metall Mater Trans A*. 1999;30:601–10.
6. Yang TQ. *The ory of viscoelasticity*. Wuhan: Huazhong University of Science and Technology Press; 1990.
7. Hu J, Sun G, Zhang X, Wang G, Jiang Z, Han S, et al. Effects of loading strain rate and stacking fault energy on nanoindentation creep behaviors of nanocrystalline Cu, Ni-20 wt.%Fe and Ni. *J Alloys Compd*. 2015;647(1):670–80.
8. Zhou PF, Xiao DH, Li G, Song M. Nanoindentation creep behavior of CoCrFeNiMn high-entropy alloy under different high-pressure torsion deformations. *J Mater Eng Perform*. 2019;28(5):2620–9.
9. Pharr GM, Oliver WC, Brotzen FR. On the generality of the relationship among contact stiffness, contact area, and elastic modulus during indentation. *J Mater Res*. 1992;7(03):613–7.
10. Yang S, Zhang YW, Zeng K. Analysis of nanoindentation creep for polymeric materials. *J Appl Phys*. 2004;95(7):3655.
11. Dirras G, Couque H, Lilensten L, Heczal A, Tingaud D, Couzinié JP, et al. Mechanical behavior and microstructure of Ti₂₀Hf₂₀Zr₂₀Ta₂₀Nb₂₀ high-entropy alloy loaded under quasi-static and dynamic compression conditions. *Mater Charact*. 2016;111:106–13.
12. Wang L, Qiao JW, Ma SG, Jiao ZM, Zhang TW, Chen G. Mechanical response and deformation behavior of Al_{0.6}CoCrFeNi high-entropy alloys upon dynamic loading. *Mater Sci Eng*. 2018;727:208–13.
13. Meyers MA. *Dynamic behavior of materials*. New York: Wiley; 1994.
14. Kassner ME. *Fundamentals of creep in metals and alloys*. London: Butterworth-Heinemann, an imprint of Elsevier; 2009.
15. Mayo MJ, Nix WDA. micro-indentation study of superplasticity in Pb, Sn, and Sn-38 wt% Pb. *Acta Metall*. 1988;36(8):2183–92.
16. Raman V, Berriche R. An investigation of the creep processes in tin and aluminum using a depth-sensing indentation technique. *J Mater Res*. 1992;7(3):627–38.
17. Oliver WC, Pharr GM. An improved technique for determining hardness and elastic modulus using load and displacement sensing indentation experiments. *J Mater Res*. 1992;7(6):1564–83.
18. Cao ZH, Li PY, Lu HM, Huang YL, et al. Indentation size effects on the creep behavior of nanocrystalline tetragonal Ta films. *Scr Mater*. 2009;60(6):415–8.
19. Wang F, Huang P, Xu KW. Time dependent plasticity at real nanoscale deformation. *Appl Phys Lett*. 2007;90(16):161921.
20. Zhang L, Yu P, Cheng H, Zhang H, Diao H, Shi Y, et al. Nanoindentation creep behavior of an Al_{0.3}CoCrFeNi high-entropy alloy. *Metall Mater Trans A*. 2016;47(12):5871–5.
21. Sun W, Jiang Y, Sun G, Hu J, Zhou T, Jiang Z, et al. Nanoindentation creep behavior and its relation to activation volume and strain rate sensitivity of nanocrystalline Cu. *Mater Sci Eng A*. 2019;751:35–41.
22. Xu Y, Zhan L, Li W. Effect of pre-strain on creep aging behavior of 2524 aluminum alloy. *J Alloys Compd*. 2017;691:564–71.
23. Song H, Yavas H, Van der Giessen R, Papanikolaou S. Discrete dislocation dynamics simulations of nanoindentation with pre-stress: hardness and statistics of abrupt plastic events. *J Mech Phys Solids*. 2018;123:332–47.

Springer Nature or its licensor holds exclusive rights to this article under a publishing agreement with the author(s) or other rightsholder(s); author self-archiving of the accepted manuscript version of this article is solely governed by the terms of such publishing agreement and applicable law.